PCCP

Accepted Manuscript

ROYAL SOCIETY OF CHEMISTRY

www.rsc.org/pccp

Physical State and Acidity of Inorganic Sulfate Can Regulate the Production of Secondary Organic Material from Isoprene Photooxidation Products

by

Mikinori Kuwata[†,§], Yingjun Liu[†], Karena McKinney[†], and Scot T. Martin[†,*]

[†] School of Engineering and Applied Sciences & Department of Earth and Planetary Sciences, Harvard University, Cambridge, Massachusetts, USA 02138

[§]Now at Division of Earth Sciences, Nanyang Technological University, Singapore, and Earth Observatory of Singapore

E-mail: scot_martin@harvard.edu

http://www.seas.harvard.edu/environmental-chemistry

Submitted: December 4, 2014

Physical Chemistry and Chemical Physics

[*]To Whom Correspondence Should be Addressed

Abstract

The production of secondary organic material (SOM) by the reactive uptake of isoprene photooxidation products was investigated using partially to wholly neutralized sulfuric acid particles. The experiments were performed at a relative humidity (RH) of < 5% and a temperature of 20 °C. The extent X of neutralization was adjusted from that of sulfuric acid (X = 0) to that of ammonium sulfate (X = 1). Significant SOM production was observed only for X < 0.7. The threshold of 0.7 corresponded to the transition point of the sulfate particles from aqueous to solid for < 5% RH. The phase transition of inorganic sulfate therefore regulated the particle-phase reactions that produce isoprene SOM, at least for the investigated conditions. For aqueous particles, a decreasing extent of neutralization was associated with increasing production of SOM, including increased production of oligomers and organosulfates. These results can underpin treatments of phase-dependent SOM production within chemical transport models, thereby improving the accuracy of simulations of biogenic-anthropogenic interactions in the atmosphere and the associated impacts of aerosol particles on climate and air quality.

Keywords: secondary organic material, isoprene photooxidation, degree of neutralization, phase, oligomers, organosulfates

1. Introduction

Biogenic volatile organic compounds are oxidized in the atmosphere, producing gas- and particle-particle products that constitute the atmospheric secondary organic aerosol. The particle-phase component comprises so-called secondary organic material (SOM).[1, 2] Atmospheric SOM production occurs by several parallel pathways, such as gas-to-particle condensation as well as multiphase reactions in cloud hydrometeors and haze particles.[1, 3-6] The production pathways, including anthropogenic-biogenic interactions, must be adequately understood and quantified to serve as a basis for accurate modeling of climate- and health-relevant properties of particles.[7, 8] An important consideration for the atmosphere is the role of sulfate particles, which are ubiquitous in the atmosphere and frequently serve as substrates for SOM production.

Isoprene is of central importance for atmospheric SOM production because of its high emissions.[9, 10] Many laboratory, field, and modeling studies have been carried out.[11-17] Several laboratory experiments have demonstrated that isoprene SOM production is enhanced in the presence of acidic sulfate particles, suggesting the role of particle-phase reactions.[18, 19] Field observations are also consistent with the importance of particle-phase reactions for isoprene SOM production.[11, 12] The physical state of sulfate particles in the troposphere can either be solid or liquid,[20] and SOM production from isoprene can be expected to depend on physical state. Although chemical transport models include the effects of physical state for some chemical reactions, such as hydrolysis of N_2O_5,[21, 22] currently available experimental data sets are not sufficient to constrain the effect of physical state on SOM production from isoprene.

Isoprene epoxydiol (IEPOX) isomers are produced in the gas phase during isoprene photooxidation and have been confirmed as one of the most important contributors to

particle-phase SOM production.[23, 24] The isomers are taken up into the particle phase and subsequently undergo acid-catalyzed reactions. The importance of IEPOX has motivated several recent laboratory studies to investigate SOM production directly from IEPOX. SOM was produced when aqueous ammonium sulfate particles were exposed to IEPOX. [25, 26] Exposure to crystalline ammonium sulfate particles, however, did not lead to SOM production. Moreover, another study[27] showed that the reactive uptake coefficient of IEPOX positively correlated with proton concentration, meaning that the acidity of sulfate particles is an important regulator of SOM production from IEPOX.

These two leading facts, namely the importance of physical state and acidity for SOM production from IEPOX, motivate the closer scrutiny in the present study of the detailed relationship between the state diagram of partially to wholly neutralized sulfate particles and isoprene SOM production. Ammonium and protons are the dominant counter ions to sulfate in most regions of the troposphere, and the ratio of ammonium and protons determines whether the sulfate is wholly or partially neutralized. The extent X of neutralization is quantified as follows: $X = 0.5 n_{NH_4^+} / n_{SO_4^{2-}}$, for n as the number of moles of ammonium or sulfate in the particle. By this definition, X ranges from highly acidic ($X \rightarrow 0$) to completely neutralized ($X \rightarrow 1$) (Figure 1). Extent of neutralization is one master variable of the physical state[28] (cf. Figure 1, Table S2[29]). The solid or liquid state also depends relative humidity (RH) as well as the relative concentrations of organics, nitrates, and other species mixed with the sulfates.[28, 30, 31]

In advance of the present study and in the context of current literature, several relationships between the state diagram of partially to wholly neutralized sulfate particles and SOM production from IEPOX could be hypothesized. SOM production from IEPOX by acidic particles might be expected to be parameterized as a continuous function of X and RH if the

availability of protons plays the key role. In contrast, a discontinuous function with *X* might be expected to describe SOM production if the phase transition plays the critical role. Another possibility is that the sensitivity to physical state and acidity for SOM production from IEPOX uptake might differ from that for the full case of isoprene photooxidation, which includes many more products than IEPOX alone.[32] The present study was undertaken to experimentally determine the validity of these possible hypotheses.

2. Experimental

A schematic diagram of the experimental setup is shown in Figure 2. Two serial reactors were used to separate gas-phase photooxidation reactions from particle-phase reactions. In the first reactor (Harvard Environmental Chamber; HEC), isoprene was photooxidized in the gas phase under conditions for which the HO_2 reaction pathway dominated over NO and RO_2 pathways.[15] Conditions were such that SOM production did not occur in the first reactor. The outflow of the gaseous reaction products from this reactor passed into a second reactor, which was a 72-L glass flask. A flow of sulfate particles of variable *X* also entered this reactor. Depending on reaction conditions SOM production occurred in the second reactor. Mass spectra of the particle phase and the gas phase were collected from the outflow of the second reactor.

2.1 Production of isoprene photooxidation products (reactor 1)

The HEC was operated as a continuously mixed flow reactor (CMFR) under steady-state conditions.[33] The flow rate was 21 Lpm, corresponding to a mean residence time of 3.7 hr. As described in ref 15, isoprene was injected from a standard cylinder (250 ppm in N_2; Scott gas specialty) through a mass flow controller, resulting in an inflow concentration of 120 ppb into the HEC. An aqueous H_2O_2 solution (31.5% w/w; TraceSELECT Ultra, Fluka) was injected into the inflow using a syringe pump. Irradiation photolyzed H_2O_2 to produce OH radicals, initiating

photochemical reactions. The particle number concentration in the HEC outflow was < 0.5 cm^{-3}, as monitored using a condensation particle counter (CPC, TSI model 3776). This concentration was low enough to confirm the absence of new particle production for the reaction conditions. The outflow isoprene concentration was 36 ppb, meaning that 84 ppb of isoprene was oxidized in the HEC.

2.2 Production of sulfate particles

A 0.01% (w/w) aqueous solution of ammonium sulfate was atomized (TSI, model 3076 atomizer) to produce aqueous aerosol particles (Figure 2). The particle flow was dried to < 5% RH using a diffusion dryer, causing the particles to crystallize.[28] The flow subsequently passed through a radioactive source (^{210}Po) to neutralize charge. A fraction of the particle population was selected by a differential mobility analyzer (DMA, TSI model 3085). The DMA was operated at sheath-to-sample flow ratio of 10:1. The central mobility diameters of +1 and +2 particles were 50 and 72 nm, respectively. They were produced in a number ratio of 2:1, corresponding to a volume ratio of 1:1. The combined number concentration was 5000 cm^{-3}.

After the DMA, the mobility-classified particles were exposed to sulfuric acid vapor. The vapor was produced by heating a concentrated solution (96% w/w) of sulfuric acid to 25 to 70 °C.[34] The mass of depositing vapor was regulated by the heater temperature, ultimately determining X of the mixed particles. The condensing liquid sulfuric acid partially to wholly dissolved the ammonium sulfate. In this way, both X and particle phase were regulated according to the state diagram of sulfate (Figure 1). No new particle production (i.e., of H_2SO_4) was observed in the number-diameter data sets. Because of the differing diameters of the +1 and +2 particles, X_{+1} was more acidic than X_{+2}, reaching up to (X_{+1} - X_{+2}) = -0.1 for X of 0.3, corresponding to the most acidic particles produced using the DMA (Table S3). Herein, the

mass-weighted value of X for the particle population, as determined by measurement of sulfate and ammonium mass concentrations by mass spectrometry, is reported. Both the uncertainty in the AMS data and the different acidities of X_{+1} and X_{+2} particles were considered in calculating the uncertainty of X.

For $X < 0.1$, the DMA voltage was turned off, meaning that no ammonium sulfate particles were injected into the glassware. The temperature of the sulfuric acid bath was increased up to 70 °C to induce new particle production, leading to concentrations of up to 10^6 cm^{-3} in the second reactor. For these experiments, adventitious NH_3 slightly neutralized the particles (i.e., $0 < X < 0.1$), as observed in the NH_4^+:SO_4^{2-} mass ratio determined by particle mass spectrometry.[35]

2.3 Mixing of isoprene photooxidation products and sulfate particles (reactor 2)

The flows of photooxidation products from the HEC and of sulfate particles from the particle generator were mixed together in a second reactor, consisting of a 72-L glass flask (Ace Glass, Inc. 6533-28). The experiment was conducted in continuous flow, and the mean residence time in the reactor was 1.4 hr. The reactor was covered in aluminum foil to avoid irradiation by laboratory lighting. The relative humidity in the reactor was < 5%, indicating that the liquid water was less than 5% (w/w) or lower, based on the water uptake of hygroscopic growth of ammonium bisulfate.[36] The reactor was capped by a head (Ace Glass, Inc. 6530) having four ports for tubing of 6.35 mm (o.d). Stainless steel tubing was used for the particle inflow. Teflon tubing was used for the gas inflow. The stainless steel and Teflon tubing were inserted into the reactor at different heights to facilitate mixing. Stainless steel tubing and Teflon tubing were also used for outflow sampling to particle and gas instrumentation, respectively. Comparison of

inflow to outflow particle concentrations indicated that 41 ± 4% of the particles were lost in the reactor 2.[37]

2.4 Characterization of reaction products

The particles in the outflow from the second reactor were sampled by a Scanning Mobility Particle Sizer (SMPS; TSI model 3936) to record the number-diameter distribution of the particle population.[38] The SMPS consisted of a DMA (TSI model 3081) and a CPC (TSI model 3776). The DMA voltage was scanned from 32 to 6358 V, corresponding to a diameter range of 25.5 to 487 nm for a sheath flow of 3.0 Lpm and a sample flow of 0.3 Lpm. The scanning time of the DMA was 100 s. The overall time resolution of the measurement was 120 s.

The particles in the outflow of the second reactor were sampled by a high-resolution time-of-flight Aerosol Mass Spectrometer (HR-ToF-AMS; Aerodyne. Inc).[39] The mass spectra were analyzed to obtain the mass concentrations of sulfate, ammonium, and organic species as well as information about the chemical composition about the organic species. Ionization was at 70 eV by electron impact, resulting in extensive fragmentation. Although the fragmentation precluded identification of specific compounds, the SOM spectra were nevertheless characteristic of different chemical types. The data analysis of the particle mass spectra incorporated updates to the fragmentation table (cf. Supporting Information).[40] The data analysis software packages *Sequential Igor Data Retrieval* (SQUIRREL ver. 1.51H) and *Peak Integration by Key Analysis* (PIKA ver. 1.10H) were employed.

Speciation of the gas-phase species was conducted using a selective-reagent-ionization time-of-flight mass spectrometer (SRI-NO^+-ToF-MS, Ionicon Analytik GmbH) using NO^+ as the reagent ion.[41] Soft chemical ionization by NO^+ (9.6 eV) resulted in one or a few product ions, and the attribution of ions to specific molecules was possible.[42] The instrument settings and data

analysis procedures of SRI-NO^+-TOF-MS were described in ref 15. Instrument sensitivity was checked periodically using isoprene and methacrolein supplied from a standard cylinder.

2.5 Injection of IEPOX isomers

For selected experiments, instead of using isoprene photooxidation products from the HEC (i.e., reactor 1), a gas flow containing one of the IEPOX isomers (*trans*-β- or δ1-IEPOX; Table S4) was injected into the second reactor. The IEPOX synthesis was described in ref [43]. Prior to an experiment, the purity of an IEPOX isomer after storage was re-confirmed by nuclear magnetic resonance (NMR) spectroscopy. For volatilization, liquid IEPOX isomer was placed inside of a Teflon T-fitting, and the fitting was flushed by purified air, thereby producing a volatilized stream of the IEPOX isomer. The liquid evaporated slowly across several days, providing a stable IEPOX source across the time period of the conducted experiments.

3. Results

3.1 Time series

Figure 3 shows a typical time series of the temperature of the sulfuric acid bath and particle mass concentrations of organic, sulfate, and ammonium species (M_{org}, M_{SO4}, and M_{NH4}, respectively). The calculated extent X of particle neutralization is also plotted. The SRI-NO^+-ToF-MS signal intensity of the $C_5H_6O^+$ ion, which is a marker for the gas-phase concentration of β-IEPOX,[15] is also shown. As described in ref [37], decreases in the concentration of β-IEPOX correlated linearly with the production of SOM.

At the beginning of the shown experiment (Figure 3), the heater for sulfuric acid was off, meaning that ammonium sulfate ($X = 1$) particles entered the second reactor. Although there was an inflow of isoprene oxidation products from the HEC, no SOM was produced in the second reactor. When the heater was turned on, M_{SO4} increased and X decreased. Corresponding

increases of M_{org} and decreases of gas-phase IEPOX were observed. The magnitude of these changes increased for higher heater temperatures. In the last step of the experiment, the DMA voltage was set to zero, meaning that no ammonium sulfate particles passed over the sulfuric acid bath. For this condition, sulfuric acid particles were produced by homogeneous nucleation of molecules volatilized from the bath, leading to the least neutralized particles ($X < 0.1$) and the highest M_{org} of the study. At the end of the experiment, the injection of sulfuric particles was terminated, and the particle concentrations decreased rapidly. The signal intensity of $C_5H_6O^+$ from gas-phase sampling, however, responded more slowly, indicative of the stickiness of IEPOX of reactor surfaces and its subsequent condensation and evaporation.

3.2 Organic particle mass spectra

Examples of the mass spectra collected for the organic component of particles in the outflow from the second reactor are shown in Figure 4 for X of 0.01 and 0.60. For comparison to these spectra, mass spectra are also shown for particle-phase organic material produced by the uptake of IEPOX isomers by less neutralized sulfate particles ($X < 0.1$). A further reference spectrum obtained from ref [44] is shown for SOM produced during isoprene photooxidation in the HEC in the presence of ammonium sulfate particles (i.e., a single reactor and using neutral, solid sulfate particles). The major ions that are present in panels *a* to *d* of Figure 4 are listed in Table 1 for $m/z < 110$ and in Table 2 for $m/z > 110$. Overall, the mass spectra for SOM produced by the uptake of isoprene photooxidation products (Figures 4a and 4b) are similar to those obtained for SOM produced by the uptake of the two IEPOX isomers in the presence of non-neutralized sulfate particles (Figures 4c and 4d). The similarity is consistent with the correlation between increasing particle-phase M_{org} and decreasing gas-phase $C_5H_6O^+$ (Figure 3), suggesting that the IEPOX family is a dominant contributor to the produced SOM.[37]

4. Discussion

4.1 Physical state of sulfate particles and SOM production

The dependence of the produced SOM mass concentration M_{org} on the extent X of neutralization is shown in Figure 5a. For $X < 0.7$, M_{org} decreases for increasing X, and SOM production becomes insignificant for $X > 0.7$. This threshold value of 0.7 is related to the solid or liquid physical state of the sulfate particles. For sufficiently low values of RH, the solids ammonium sulfate ($X_{solid} = 1.0$; AS) and letovicite ($X_{solid} = 0.75$; LET) crystallize from aqueous solution for $X > 0.7$ (Figure 1). By comparison, for submicron particles at room temperature the solid ammonium bisulfate ($X_{solid} = 0.5$; AHS) does not crystallize from aqueous solution by homogeneous nucleation even at low RH, meaning that the liquid state is metastable.[29, 45, 46] The implication for the present study is that the aqueous sulfate particles of $X < 0.6$ do not crystallize. For $0.6 < X < 0.7$, within a population of particles, some individual sulfate particles can crystallize completely as two crystals (i.e., LET +AHS) whereas others can remain aqueous.[47, 48] For $X > 0.7$, all particles in the population crystallize.[48] The data set of Figure 5a for the dependence of M_{org} on X, in conjunction with the dependence of phase on X, leads to the inference that SOM production is greatly inhibited in the presence of solid compared to aqueous particles.[49]

An alternative presentation of the results is shown in Figure 5b. Literature results suggest that isoprene SOM production correlates with proton concentration.[19] For the present experiments, this possibility is explored by using the quantity M_{org}/M_{H2SO4} as the ordinate Figure 5b in place of M_{org} as the ordinate in Figure 5a. As for the plot of M_{org} with X (Figure 5a), the plot of M_{org}/M_{H2SO4} with X (Figure 5b) shows a threshold point for $X < 0.7$, which is related to the solid or liquid state of the sulfate particles. For a counter hypothesis that the reactions might

be limited entirely by the stoichiometry of excess sulfuric acid, the plot of Figure 5b would then be anticipated as a horizontal line for $X < 0.7$. The data in the figure, however, do not support this explanation.

Several explanations for the observed behavior can be considered. One possibility is a kinetic limitation. According to this hypothesis, the reactions proceed faster for lower X (e.g., acid catalyzed), and greater M_{org} is therefore observed for lower X. The implication of this hypothesis is that the reactions do not go to completion within the residence time in reactor 2, meaning that additional particle growth ought to be observed for additional residence time. The experimental observation, however, is that the particle number-diameter distribution does not change after turning off the inflow of sulfate particles (Figure S2). The implication of this counter observation is that the reactions go to completion within the residence time of the reactor.

The observed behavior of Figure 5b can be explained by consideration of the turnover number for the catalytic reactions by proton to produce SOM from IEPOX, meaning that the reactive uptake of IEPOX molecules is limited by the number of protons. Protons, both as hydronium H_3O^+ and bisulfate HSO_4^- ions, are catalytic acidic agents for ring-opening reactions of epoxides as well as further reactions in the condensed phase.[50] The reactions series of SOM production therefore consists of initiation, propagation, and termination steps, and the reaction series is characterized by a turnover number for proton species. According to this explanation, the implication of the data set of Figure 5b is that the turnover number is higher for lower X.

The turnover number can be calculated from M_{org}/M_{H2SO4}, as follows. Prototypical particle-phase products from IEPOX uptake and oxidation include non-sulfate species such as methyl tetrol ($C_5H_{12}O_4$, 0.136 kg mol^{-1}) and organosulfates such as trihydroxy methyl

hydrogensulfate (formula $C_5H_{12}O_7S$; 0.119 kg mol^{-1} as organic + 0.097 kg mol^{-1} as sulfate; the AMS detects only the organic portion as part of M_{org}). As an assumption for further development of the analysis, the average of these two values (0.128 kg mol^{-1}) is taken as the average molecular weight of the SOM monomeric products. In this case, $M_{org}/M_{H2SO4} = 2.7$ for a turnover number of 1, considering that one sulfuric acid molecule contains two protons. The value of M_{org}/M_{H2SO4} varies from 3 for X approaching 0.7 to 12 for $X < 0.5$, which corresponds to an enhancement of turn over number of proton from 1.1 to 4.5. The turnover number could be a useful constraint in chemical transport models for isoprene SOM production by particle-phase reactions, especially at times of limited available excess sulfate.

4.2 Oligomers and Organosulfates

Table 2 provides a list of significant ions that consist of six or more carbon atoms based on the high-resolution *m*/*z* values. Isoprene, as the reactant molecule, comprises five carbon atoms, suggesting that the ions in Table 2 arise from oligomers. Of these, the signal at *m*/*z* 129.0552 ($C_6H_9O_3^+$) is the strongest. Figure 6a shows the dependence of the relative intensity (i.e., the fraction of the AMS organic mass spectrum) of this signal on X. Results similar to those in Figure 6a are observed for other significant oligomer ions (e.g., $C_5H_7O_3^+$ at *m/z* 115.0394 and $C_5H_9O_3^+$ at *m/z* 117.0551; Figure S3). The implication of these results is that the overall oligomer fraction in the produced SOM increases for smaller X, consistent with the fact that many oligomer production processes are acid-catalyzed.[24, 50]

Figure 6b shows the dependence of the relative intensity of *m*/*z* 136.9909 ($C_3H_5SO_4^+$) on the X. Based on the high-resolution *m*/*z* value, the conclusion is that this ion derives from an organosulfate species. Of the several ions present in the mass spectrum for organosulfates for *m*/*z* > 110, this ion is the most intense (Table 2). As for the oligomer signals, the organosulfate

fraction increases for decreasing X, and the organosulfate and oligomer fractions correlate linearly (Figure S4; $R^2 = 0.90$). This correlation might be explained by several possibilities. One possibility is that oligomer and organosulfate production both follow acid-catalyzed reaction pathways, making proton concentration a common governing variable of both reaction pathways. Another possibility is that the sulfate moiety in the organosulfate is a linking unit of the oligomers so that the AMS is detecting fragment ions originating from the same compound.

4.3 Comparison to single-reactor configuration

An example of a mass spectrum of SOM produced by isoprene photooxidation in a single-reactor configuration at 40% RH with solid sulfate particles is shown in panel *e* of Figure 4,[44] and can be compared with the mass spectra shown in panels *a* and *b* (two reactor configuration; this study). The reaction conditions of the two studies are similar with respect to initial precursor concentration (200 ppb isoprene for the previous study) and photooxidation conditions, although the RH values of the two studies differ (i.e., <5% for panels *a* and *b* and 40% RH for panel *e*). Comparison of the mass spectra shows that there are significant differences. For instance, major peaks at *m/z* 53, 82, and 101 in panels *a* and *b* are not significant in panel *e*, implying that the SOM composition differs. The intensities of possible oligomer signals for *m*/*z* > 110 are also significantly reduced, demonstrating less occurrence of oligomerization. The fraction of signal at *m*/*z* 82, which has been used as a tracer ion for isoprene photooxidation products in some field studies,[11, 17] is an order of magnitude less in panel *e* compared to panels *a* and *b*.

Given that the mass spectra of SOM derived directly from IEPOX isomers (i.e., panels *c* and *d*) are similar to those of the SOM produced in the present study using acidic particles (i.e., panels *a* and *b*), the implication by comparison to panel *e* is that these IEPOX compounds

contribute negligibly to SOM production for the conditions of panel *e*, i.e., solid particles. This conclusion is also consistent with the findings of ref 24 that compounds traceable to IEPOX compounds by chromatographic analyses are present when acidic particles are used but are not significant when neutral particles are employed. Moreover, the particle mass yield of ref [44] is (5 ± 3)% for solid particles whereas it is as high as (26 ± 2)% in the present study for acidic aqueous particles ($X < 0.1$). The difference in yields further supports a primary role of particle-phase reactions for SOM production under atmospheric conditions during time periods when aqueous particles are present.

The absence of significant SOM production in the presence of fully neutralized sulfate particles (i.e., $X = 1$) for the two-reactor configuration of the present study differs from the substantial production observed previously in a combined-reactor configuration.[44] Some possible explanations are loss to the walls of low-volatility compounds in the transfer lines from the first to the second reactor or the absence of photochemistry in the second reactor (i.e., implying a need for particle surface area in the presence of irradiation for SOM production). A full understanding of the differences between the two sets of experiments requires further research.

5. Conclusions and atmospheric implications

The physical state of atmospheric particles can fluctuate between solid and liquid depending on local and prior relative humidity, particle composition, and other factors.[20, 31, 51] The current study finds that there is a discontinuous function in the produced SOM mass concentration at a threshold value of 0.70 for *X*, at least for low RH. The implication is that an aqueous phase is needed for isoprene SOM production by particle-phase reactions. Moreover, isoprene SOM production, the oligomer fraction, and the organosulfate fraction all steadily increase for increasingly acidic particles. Chemical transport models of atmospheric organic

mass concentration have begun to simulate isoprene SOM production from the reactive uptake of known photooxidation products, such as the IEPOX family.[14, 16] The current experimental results imply that updated models should also treat the physical state and the extent of neutralization of the reactive medium. The present study was limited to <5% RH, and future laboratory studies to continue to investigate the role of relative humidity are well motivated. Experiments at higher RH are especially useful in quantifying the relative importance of physical state and humidity for particle-phase SOM production. Furthermore, investigation of the roles of other materials such as inorganic-organic mixtures and semi-solid organic materials on isoprene SOM formation are needed. [30, 34]These future studies can be combined toward an eventual objective of the parameterization of the effects of the physical state, acidity, and humidity on SOM production from isoprene.

Acknowledgments

This material is based upon work supported by the Office of Science (BES), U.S. Department of Energy, Grant No. DE-FG02-08ER64529 and by the National Science Foundation, Grant No. 1249565 and 0959452. Y.J.L. is supported by NASA Earth and Space Science Fellowship Program. M.K. was supported by the Japan Society for the Promotion of Science Fellowship for Research Abroad when the study was conducted. We acknowledge B.F. Strick, R.J. Thomson, and F.M. Geiger (Northwestern University) for synthesizing IEPOX compounds, as described in ref [37].

References

1. M. Hallquist, J. C. Wenger, U. Baltensperger, Y. Rudich, D. Simpson, M. Claeys, J. Dommen, N. M. Donahue, C. George, A. H. Goldstein, J. F. Hamilton, H. Herrmann, T.

Hoffmann, Y. Iinuma, M. Jang, M. E. Jenkin, J. L. Jimenez, A. Kiendler-Scharr, W. Maenhaut, G. McFiggans, T. F. Mentel, A. Monod, A. S. H. Prevot, J. H. Seinfeld, J. D. Surratt, R. Szmigielski and J. Wildt, *Atmos. Chem. Phys.*, 2009, **9**, 5155-5236.

2. V. Ramanathan, M. V. Ramana, G. Roberts, D. Kim, C. Corrigan, C. Chung and D. Winker, *Nature*, 2007, **448**, 575-578.
3. Q. Chen, Y. Liu, N. M. Donahue, J. E. Shilling and S. T. Martin, *Environ. Sci. Technol.*, 2011, **45**, 4763-4770.
4. M. Kuwata and S. T. Martin, *Aerosol Sci. Technol.*, 2012, **46**, 937-949.
5. M. Shiraiwa, L. D. Yee, K. A. Schlling, C. L. Loza, J. S. Craven, A. Zuend, P. J. Ziemann and J. H. Seinfeld, *PNAS*, 2013, **110** 11746–11750.
6. A. Zuend and J. H. Seinfeld, *Atmos. Chem. Phys.*, 2012, **12**, 3857-3882.
7. A. H. Goldstein, C. D. Koven, C. L. Heald and I. Y. Fung, *PNAS*, 2009, **106**, 8835-8840.
8. A. Setyan, Q. Zhang, M. Merkel, W. B. Knighton, Y. Sun, C. Song, J. E. Shilling, T. B. Onasch, S. C. Herndon, D. R. Worsnop, J. D. Fast, R. A. Zaveri, L. K. Berg, A. Wiedensohler, B. A. Flowers, M. K. Dubey and R. Subramanian, *Atmos. Chem. Phys.*, 2012, **12**, 8131-8156.
9. A. Guenther, C. N. Hewitt, D. Erickson, R. Fall, C. Geron, T. Graedel, P. Harley, L. Klinger, M. Lerdau, W. A. McKay, T. Pierce, B. Scholes, R. Steinbrecher, R. Tallamraju, J. Taylor and P. Zimmerman, *J. Geophys. Res.*, 1995, **100**, 8873-8892.
10. C. L. Heald, D. K. Henze, L. W. Horowitz, J. Feddema, J. F. Lamarque, A. Guenther, P. G. Hess, F. Vitt, J. H. Seinfeld, A. H. Goldstein and I. Fung, *J. Geophys. Res.*, 2008, **113**, D05211.
11. S. H. Budisulistiorini, M. R. Canagaratna, P. L. Croteau, W. J. Marth, K. Baumann, E. S. Edgerton, S. L. Shaw, E. M. Knipping, D. R. Worsnop, J. T. Jayne, A. Gold and J. D. Surratt, *Environ. Sci. Technol.*, 2013, **47**, 5686−5694.
12. M. Claeys, B. Graham, G. Vas, W. Wang, R. Vermeylen, V. Pashynska, J. Cafmeyer, P. Guyon, M. O. Andreae, P. Artaxo and W. Maenhaut, *Science*, 2004, **303**, 1173-1176.
13. J. D. Surratt, S. M. Murphy, J. H. Kroll, N. L. Ng, L. Hildebrandt, A. Sorooshian, R. Szmigielski, R. Vermeylen, W. Maenhaut, M. Claeys, R. C. Flagan and J. H. Seinfeld, *J. Phys. Chem. A*, 2006, **110**, 9665-9690.
14. G. Lin, J. E. Penner, S. Sillman, D. Taraborrelli and J. Lelieveld, *Atmos. Chem. Phys.*, 2012, **12**, 4743-4774.
15. Y. Liu, I. Herdlinger-Blatt, K. A. McKinney and S. T. Martin, *Atmos. Chem. Phys.*, 2013, **13**, 5715-5730.
16. H. O. T. Pye, R. W. Pinder, I. R. Piletic, Y. Xie, S. L. Capps, Y.-H. Lin, J. D. Surratt, Z. Zhang, A. Gold, D. J. Luecken, W. T. Hutzell, M. Jaoui, J. H. Offenberg, T. E. Kleindienst, M. Lewandowski and E. O. Edney, *Environ. Sci. Technol.*, 2013, **47**, 11056–11064.
17. N. H. Robinson, J. F. Hamilton, J. D. Allan, B. Langford, D. E. Oram, Q. Chen, K. Docherty, D. K. Farmer, J. L. Jimenez, M. W. Ward, C. N. Hewitt, M. H. Barley, M. E. Jenkin, A. R. Rickard, S. T. Martin, G. McFiggans and H. Coe, *Atmos. Chem. Phys.*, 2011, **11**, 1039-1050.
18. M. S. Jang, N. M. Czoschke, S. Lee and R. M. Kamens, *Science*, 2002, **298**, 814-817.
19. J. D. Surratt, M. Lewandowski, J. H. Offenberg, M. Jaoui, T. E. Kleindienst, E. O. Edney and J. H. Seinfeld, *Environ. Sci. Technol.*, 2007, **41**, 5363-5369.

20. S. T. Martin, H. M. Hung, R. J. Park, D. J. Jacob, R. J. D. Spurr, K. V. Chance and M. Chin, *Atmos. Chem. Phys.*, 2004, **4**, 183-214.
21. W. L. Chang, P. V. Bhave, S. S. Brown, N. Riemer, J. Stutz and D. Dabdub, *Aerosol Sci. Technol.*, 2011, **45**, 665-695.
22. J. M. Davis, P. V. Bhave and K. M. Foley, *Atmos. Chem. Phys.*, 2008, **8**, 5295-5311.
23. F. Paulot, J. D. Crounse, H. G. Kjaergaard, A. Kuerten, J. M. St Clair, J. H. Seinfeld and P. O. Wennberg, *Science*, 2009, **325**, 730-733.
24. J. D. Surratt, A. W. H. Chan, N. C. Eddingsaas, M. Chan, C. L. Loza, A. J. Kwan, S. P. Hersey, R. C. Flagan, P. O. Wennberg and J. H. Seinfeld, *PNAS*, 2010, **107**, 6640-6645.
25. T. B. Nguyen, M. M. Coggon, K. H. Bates, X. Zhang, R. H. Schwantes, K. A. Schilling, C. L. Loza, R. C. Flagan, P. O. Wennberg and J. H. Seinfeld, *Atmos. Chem. Phys.*, 2014, **14**, 3497-3510.
26. Y.-H. Lin, S. H. Budisulistiorini, K. Chu, R. A. Siejack, H. Zhang, M. Riva, Z. Zhang, A. Gold, K. E. Kautzman and J. D. Surratt, *Environ. Sci. Technol.*, 2014, **Article ASAP**.
27. C. J. Gaston, T. P. Riedel, Z. Zhang, A. Gold, J. D. Surratt and J. A. Thornton, *Environ. Sci. Technol.*, 2014, **48**, 11178–11186.
28. S. T. Martin, *Chem. Rev.*, 2000, **100**, 3403-3453.
29. S. T. Martin, J. C. Schlenker, A. Malinowski, H. M. Hung and Y. Rudich, *Geophys. Res. Lett.*, 2003, **30**, GL017930.
30. A. K. Bertram, S. T. Martin, S. J. Hanna, M. L. Smith, A. Bodsworth, Q. Chen, M. Kuwata, A. Liu, Y. You and S. R. Zorn, *Atmos. Chem. Phys.*, 2011, **11**, 10995-11006.
31. Y. You, L. Renbaum-Wolff, M. Carreras-Sospedra, S. J. Hanna, N. Hiranuma, S. Kamal, M. L. Smith, X. L. Zhang, R. J. Weber, J. E. Shilling, D. Dabdub, S. T. Martin and A. K. Bertram, *PNAS*, 2012, **109**, 13188-13193.
32. A. G. Carlton, C. Wiedinmyer and J. H. Kroll, *Atmos. Chem. Phys.*, 2009, **9**, 4987-5005.
33. J. E. Shilling, Q. Chen, S. M. King, T. Rosenoern, J. H. Kroll, D. R. Worsnop, K. A. McKinney and S. T. Martin, *Atmos. Chem. Phys.*, 2008, **8**, 2073-2088.
34. M. Kuwata and S. T. Martin, *PNAS*, 2012, **109**, 17354-17359.
35. G. Biskos, P. R. Buseck and S. T. Martin, *J. Aerosol Sci*, 2009, **40**, 338-347.
36. I. N. Tang and H. R. Munkelwitz, *J. Geophys. Res.*, 1994, **99**, 18801-18808.
37. Y. Liu, M. Kuwata, B. F. Strick, F. M. Geiger, R. J. Thomson, K. A. McKinney and S. T. Martin, accepted.
38. S. C. Wang and R. C. Flagan, *Aerosol Sci. Technol.*, 1990, **13**, 230-240.
39. P. F. DeCarlo, J. R. Kimmel, A. Trimborn, M. J. Northway, J. T. Jayne, A. C. Aiken, M. Gonin, K. Fuhrer, T. Horvath, K. S. Docherty, D. R. Worsnop and J. L. Jimenez, *Anal. Chem.*, 2006, **78**, 8281-8289.
40. J. D. Allan, A. E. Delia, H. Coe, K. N. Bower, M. R. Alfarra, J. L. Jimenez, A. M. Middlebrook, F. Drewnick, T. B. Onasch, M. R. Canagaratna, J. T. Jayne and D. R. Worsnop, *J. Aerosol Sci*, 2004, **35**, 909-922.
41. A. Jordan, S. Haidacher, G. Hanel, E. Hartungen, L. Maerk, H. Seehauser, R. Schottkowsky, P. Sulzer and T. D. Maerk, *Int. J. Mass spectrom.*, 2009, **286**, 122-128.
42. D. Smith and P. Spanel, *Mass Spectrom. Rev.*, 2005, **24**, 661-700.
43. C. J. Ebben, B. F. Strick, M. A. Upshur, H. M. Chase, J. L. Achtyl, R. J. Thomson and F. M. Geiger, *Atmos. Chem. Phys.*, 2014, **14**, 2303-2314.
44. M. Kuwata, S. R. Zorn and S. T. Martin, *Environ. Sci. Technol.*, 2012, **46**, 787-794.

45. D. J. Cziczo, J. B. Nowak, J. H. Hu and J. P. D. Abbatt, *J. Geophys. Res.*, 1997, **102**, 18843-18850.
46. I. N. Tang and H. R. Munkelwitz, *J. Geophys. Res.*, 1994, **99**, 18801-18808.
47. A. L. Mifflin, M. L. Smith and S. T. Martin, *PCCP*, 2009, **11**, 10095-10107.
48. J. C. Schlenker and S. T. Martin, *J. Phys. Chem. A*, 2005, **109**, 9980-9985.
49. A. R. Ravishankara, *Science*, 1997, **276**, 1058-1065.
50. N. C. Eddingsaas, D. G. VanderVelde and P. O. Wennberg, *J. Phys. Chem. A*, 2010, **114**, 8106-8113.
51. S. T. Martin, T. Rosenoern, Q. Chen and D. R. Collins, *Geophys. Res. Lett.*, 2008, **35**.
52. N. M. Czoschke, M. Jang and R. M. Kamens, *Atmos. Environ.*, 2003, **37**, 4287-4299.
53. J. H. Kroll, N. L. Ng, S. M. Murphy, R. C. Flagan and J. H. Seinfeld, *Geophys. Res. Lett.*, 2005, **32**, L18808.
54. N. L. Ng, A. J. Kwan, J. D. Surratt, A. W. H. Chan, P. S. Chhabra, A. Sorooshian, H. O. T. Pye, J. D. Crounse, P. O. Wennberg, R. C. Flagan and J. H. Seinfeld, *Atmos. Chem. Phys.*, 2008, **8**, 4117-4140.
55. T. E. Kleindienst, M. Lewandowski, J. H. Offenberg, M. Jaoui and E. O. Edney, *Atmos. Chem. Phys.*, 2009, **9**, 6541-6558.
56. P. S. Chhabra, R. C. Flagan and J. H. Seinfeld, *Atmos. Chem. Phys.*, 2010, **10**, 4111-4131.
57. M. Jaoui, E. W. Corse, M. Lewandowski, J. H. Offenberg, T. E. Kleindienst and E. O. Edney, *Atmos. Environ.*, 2010, **44**, 1798-1805.
58. H. Zhang, J. D. Surratt, Y. H. Lin, J. Bapat and R. M. Kamens, *Atmos. Chem. Phys.*, 2011, **11**, 6411-6424.

List of Figures

Figure 1. Scatter plot of extent X of neutralization and relative humidity for experimental studies of isoprene SOM production: ([13, 18, 19, 24, 31, 44, 52-58]13, 18, 19, 24, 31, 43, 51-57[13, 18, 19, 24, 31, 43, 51-57]13, 18, 19, 24, 31, 43, 51-57[13, 18, 19, 23, 30, 42, 51-57]●) Jang et al.,[18] (◂) Surratt et al.,[19] (◥) Surratt et al.,[24] (◆) Harvard Environmental Chamber,[31, 44] (■) Czoschke et al.,[52] (▲) Kroll et al.,[53] (▼) Surratt et al.,[13] (◥) Ng et al.,[54] (▸) Kleindienst et al.,[55] (◤) Chhabra et al.,[56] (◢) Jaoui et al.,[57] (▪) Zhang et al.,[58] and (+) Lin et al. [26] Red circles correspond to the experiments of the present study. Lines show (i) the crystallization relative humidity (CRH) of partially neutralized aqueous sulfate particles and (ii) the full deliquescence relative humidity (DRH) of particles having one or more solids in quantities and types defined by the lever rule.[48] Solids include ammonium bisulfate AHS (X_{solid} = 0.5), letovicite LET (X_{solid} = 0.75), and ammonium sulfate AS (X_{solid} = 1.0).

Figure 2. Experimental setup. Abbreviations: condensation particle counter (CPC), epoxydiol (IEPOX) isomers, diffusion dryer (DD), differential mobility analyzer (DMA), scanning mobility particle sizer (SMPS), high-resolution time-of-flight Aerosol Mass Spectrometer (HR-ToF-AMS), selective-reagent-ionization time-of-flight mass spectrometer (SRI-NO^+-ToF-MS).

Figure 3. Example of a time series of quantities measured in the outflow of reactor 2 unless noted otherwise. (a) Heater temperature of the sulfuric acid bath. (b) Organic particle mass concentration M_{org} measured by the AMS. (c) Intensity of the $C_5H_6O^+$ ion measured by the SRI-NO^+-ToF-MS. (d) Sulfate mass concentration M_{SO4} measured by the AMS. (e) Ammonium mass concentration M_{NH4} measured by the AMS. (f)

Extent X of neutralization calculated based on sulfate and ammonium concentrations. Data acquisition by the AMS was suspended because of a technical issue after 75 hr.

Figure 4. Examples of organic mass spectra recorded by the AMS. (a) SOM produced in reactor 2 by mixing a flow of gas-phase isoprene photooxidation products from reactor 1 with an aerosol flow of acidic sulfate particles (X = 0.6). (b) Same as panel *a* using more acidic sulfate particles (X = 0.01). (c) SOM produced in reactor 2 by mixing flows of *trans*-β-IEPOX isomer with acidic sulfate particles (X = 0.05). (d) SOM produced in reactor 2 by mixing flows of δ1-IEPOX isomer with acidic sulfate particles (X = 0.02). (e) Ref [44]: SOM produced in the HEC during isoprene photooxidation in the presence of ammonium sulfate particles for a single-reactor configuration and using solid ammonium sulfate particles (X = 1). In all panels, at m/z 110 there is a change in the ordinate scale of 100×.

Figure 5. Dependence of the organic particle mass concentration M_{org} produced in reactor 2 on the extent X of neutralization of the sulfate particles. (a) The ordinate is the organic particle mass concentration. (b) The ordinate is the organic particle mass concentration normalized to the acidic sulfate mass concentration. M_{H2SO4} is calculated as $(98/96M_{SO4}) - (98/36)M_{NH4}$, meaning that M_{H2SO4} corresponds to the excess relative to ammonium sulfate.

Figure 6. Dependence of the signal fraction of specific m/z values of the AMS organic mass spectrum on the extent X of neutralization. (a) Signal at m/z 129.0552 ($C_6H_9O_3^+$) associated with oligomers. (b) Signal at m/z 136.9909 ($C_3H_5SO_4^+$) associated with organosulfates.

Table 1. Significant ions for low *m*/*z* (i.e., *m*/*z* < 110) present in all of panels *a* to *d* of Figure 4.

m/*z* (unit mass resolution)	*m*/*z* (high resolution)	Ion
27	27.0235	$C_2H_3^+$
28	27.9949	CO^+
	28.0313	$C_2H_4^+$
29	29.0027	CHO^+
	29.0391	$C_2H_5^+$
39	39.0235	$C_3H_3^+$
41	41.0027	C_2HO^+
	41.0391	$C_3H_5^+$
43	43.0184	$C_2H_3O^+$
	43.0548	$C_3H_7^+$
44	43.9898	CO_2^+
	44.0262	$C_2H_4O^+$
53	53.0391	$C_4H_5^+$
55	55.0184	$C_3H_3O^+$
	55.0548	$C_4H_7^+$
81	81.0340	$C_5H_5O^+$
82	82.0419	$C_5H_6O^+$
101	101.0603	$C_5H_9O_2^+$

Table 2. Significant ions for high *m*/*z* (i.e., *m*/*z* > 110) present in all of panels *a* to *d* of Figure 4.

m/*z* (unit mass resolution)	*m*/*z* (high resolution)	ion
111	110.9905	$C_5H_3OS^+$
	111.0446	$C_6H_7O_2^+$
	111.0810	$C_7H_{11}O^+$
113	113.0603	$C_6H_9O_2^+$
114	114.0139	$C_5H_6OS^+$
115	115.0395	$C_5H_7O_3^+$
	115.0548	$C_9H_7^+$
	115.0759	$C_6H_{11}O_2^+$
117	117.0552	$C_5H_9O_3^+$
	117.0704	$C_9H_9^+$,
119	119.0497	$C_8H_7O^+$
	119.0708	$C_5H_{11}O_3^+$
	119.0861	$C_9H_{11}^+$,
127	127.0395	$C_6H_7O_3^+$
	127.0759	$C_7H_{11}O_2^+$,
129	129.0552	$C_6H_9O_3^+$
	129.0704	$C_{10}H_9^+$,
131	131.0497	$C_9H_7O^+$
	131.0708	$C_6H_{11}O_3^+$
	131.0861	$C_{10}H_{11}^+$
135	134.9752	$C_3H_3O_4S^+$
137	136.9909	$C_3H_5O_4S^+$
	137.0603	$C_8H_9O_2^+$,
	137.0966	$C_9H_{13}O^+$,
138	137.9987	$C_3H_6O_4S^+$
143	143.0708	$C_7H_{11}O_3^+$
	143.0861	$C_{11}H_{11}^+$
145	145.0501	$C_6H_9O_4^+$
	145.0653	$C_7H_{13}O_3^+$
	145.0865	$C_{10}H_9O^+$
147	147.0657	$C_6H_{11}O_4^+$
	147.0810	$C_{10}H_{11}O^+$
163	163.0065	$C_5H_7O_4S^+$
167	167.0014	$C_4H_7O_5S$

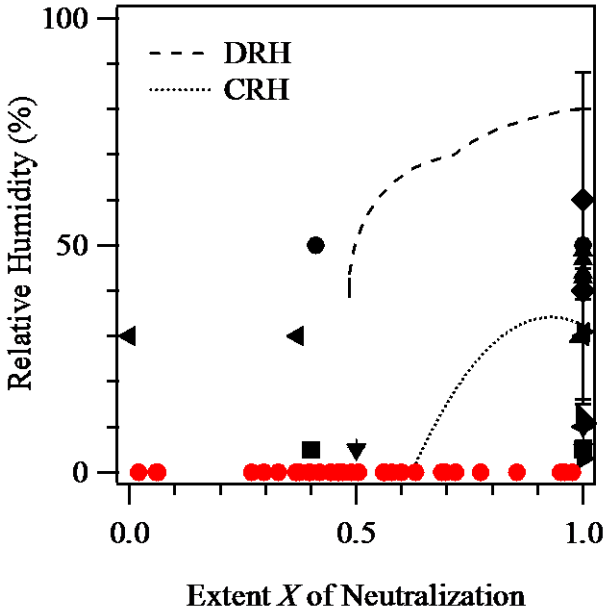

Figure 1

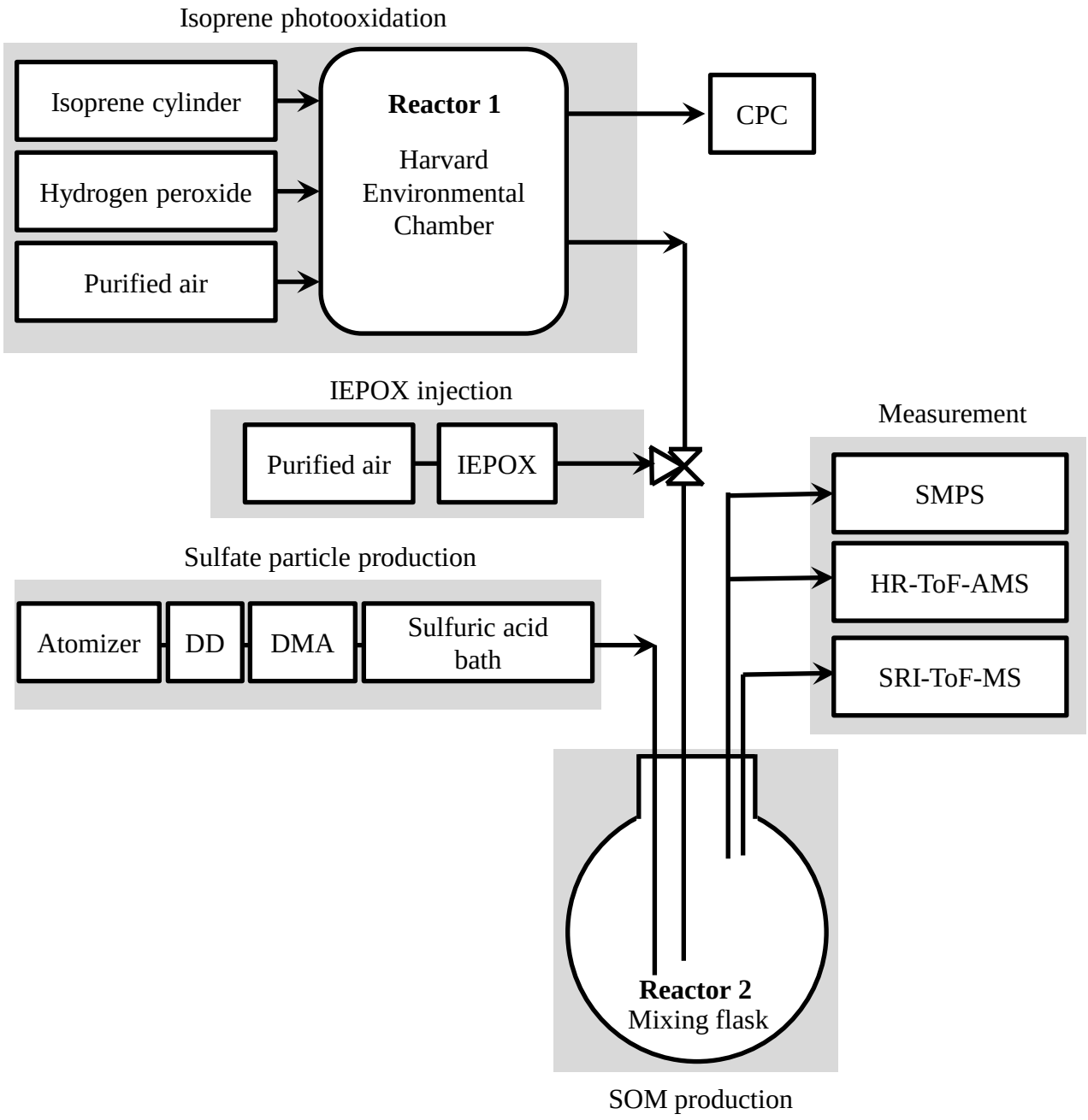

Figure 2

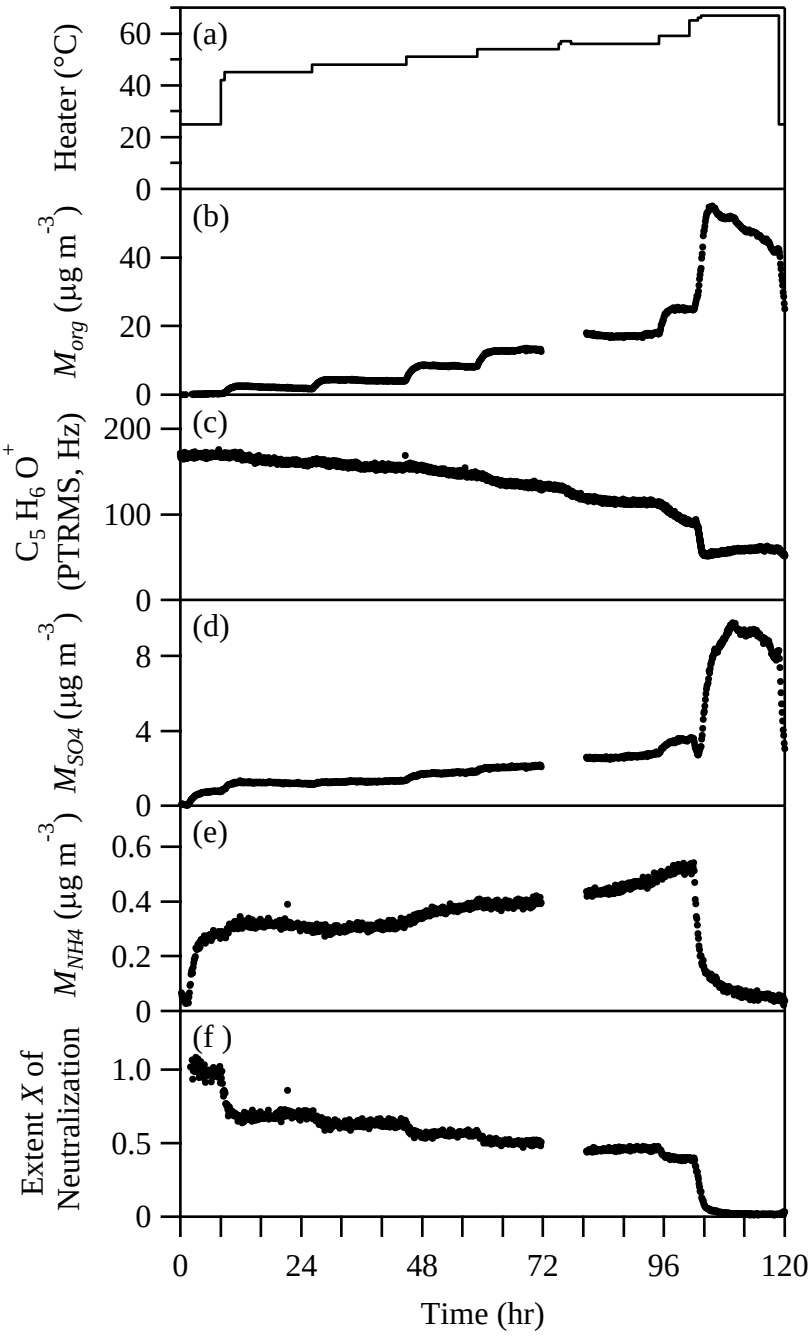

Figure 3

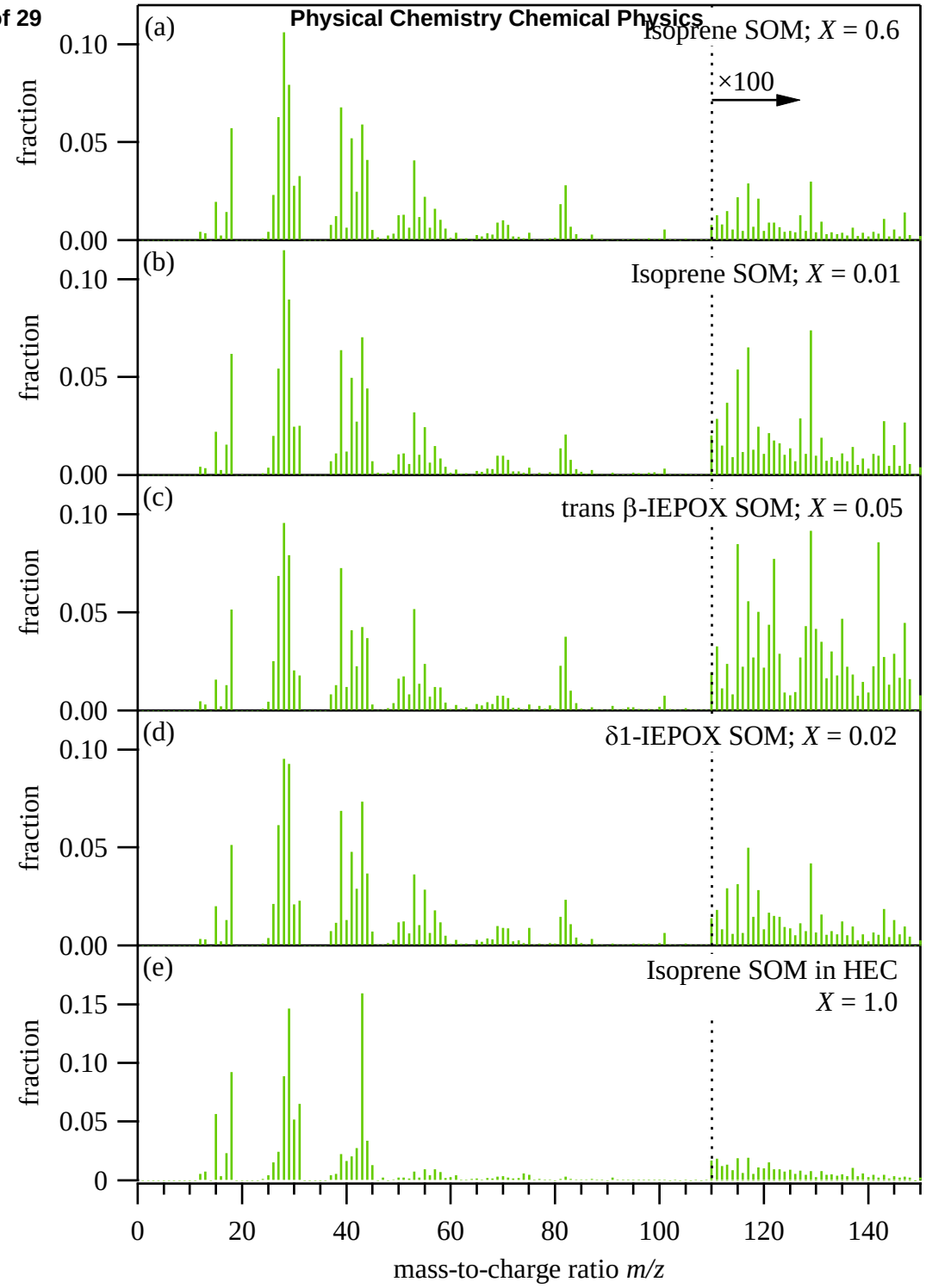

Figure 4

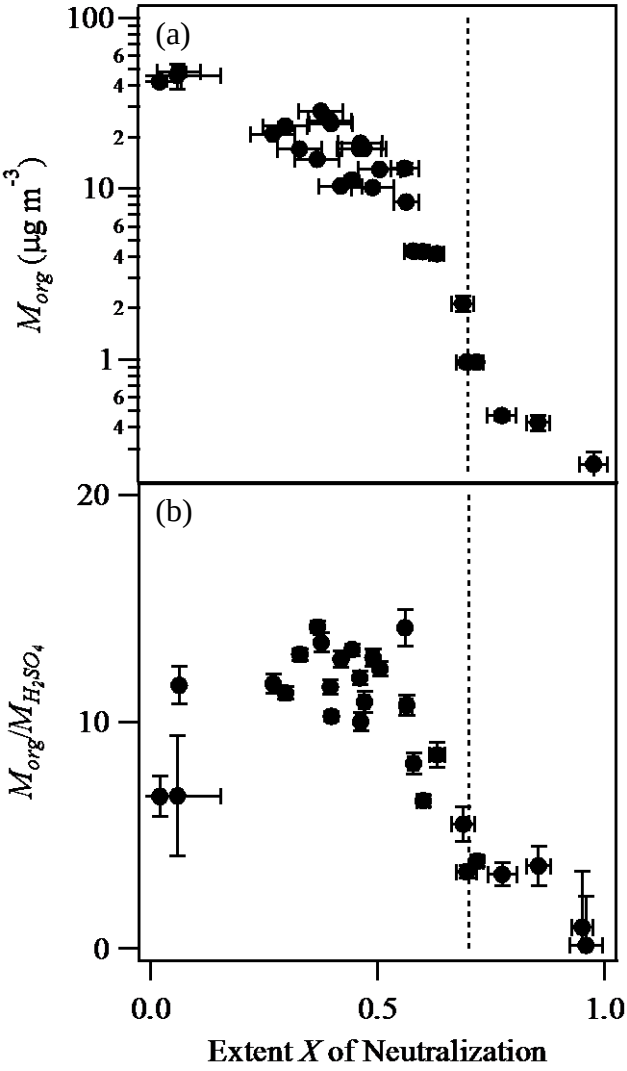

Figure 5

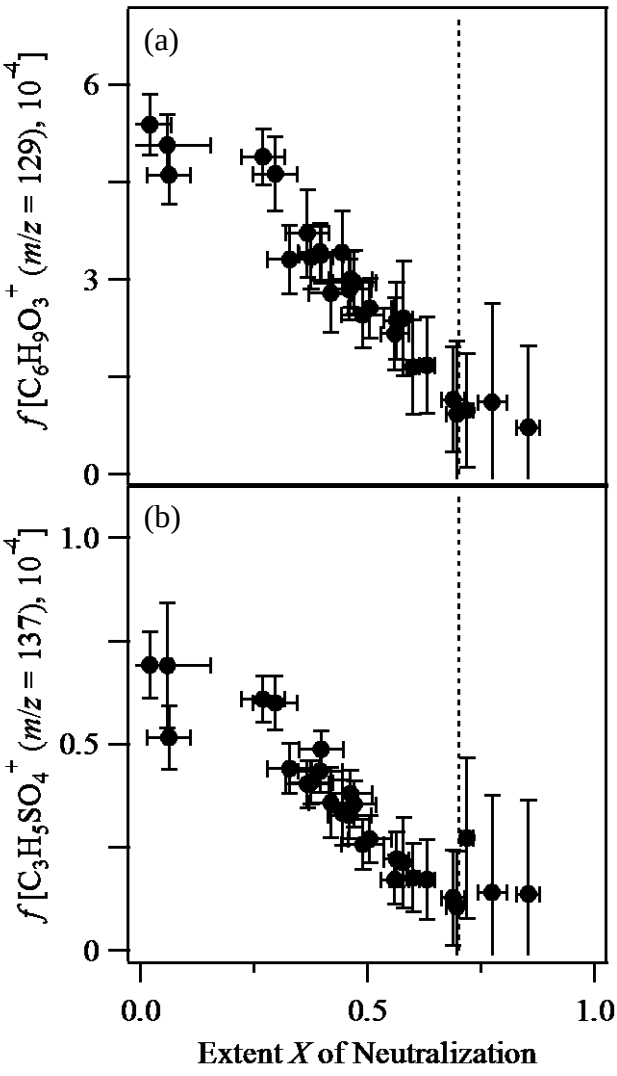

Figure 6